The *XX*-model with boundaries: III. Magnetization profiles and boundary bound states

2000 J. Phys. A: Math. Gen. 33 7661

(http://iopscience.iop.org/0305-4470/33/43/301)

J. Phys. A: Math. Gen. **33** (2000) 7661–7686. Printed in the UK PII: S0305-4470(00)13716-3

The *XX*-model with boundaries: III. Magnetization profiles and boundary bound states

Ulrich Bilstein

Universität Bonn, Physikalisches Institut, Nußallee 12, D-53115 Bonn, Germany

E-mail: bilstein@th.physik.uni-bonn.de

Received 3 May 2000

Abstract. We calculate the magnetization profiles of the σ_j^x- and σ_j^z-operators for the *XX*-model with Hermitian boundary terms. We study the profiles on the finite chain and in the continuum limit. The results are discussed in the context of conformal invariance. We also discuss boundary excitations and their effect on the magnetization profiles.

1. Introduction

We continue our study of the *XX*-model with boundaries defined by the Hamiltonian

$$H = \tfrac{1}{2}\sum_{j=1}^{L-1}[\sigma_j^+\sigma_{j+1}^- + \sigma_j^-\sigma_{j+1}^+] + \frac{1}{\sqrt{8}}[\alpha_-\sigma_1^- + \alpha_+\sigma_1^+ + \alpha_z\sigma_1^z + \beta_+\sigma_L^+ + \beta_-\sigma_L^- + \beta_z\sigma_L^z] \tag{1}$$

where $\sigma_j^{\pm} = \frac{1}{2}(\sigma_j^x \pm \mathrm{i}\sigma_j^y)$. By σ^x, σ^y and σ^z we denote the Pauli matrices. Since we restrict ourselves to Hermitian boundary terms, the values of α_z and β_z are real numbers and α_+ and β_+ are the complex conjugates of α_- and β_- respectively. In the first publication [1] of this series we have shown how to diagonalize H by introducing an auxiliary Hamiltonian

$$H_{\mathrm{long}} = \tfrac{1}{2}\sum_{j=1}^{L-1}[\sigma_j^+\sigma_{j+1}^- + \sigma_j^-\sigma_{j+1}^+] + \frac{1}{\sqrt{8}}[\alpha_-\sigma_0^x\sigma_1^- + \alpha_+\sigma_0^x\sigma_1^+ + \alpha_z\sigma_1^z + \beta_+\sigma_L^+\sigma_{L+1}^x + \beta_-\sigma_L^-\sigma_{L+1}^x + \beta_z\sigma_L^z] \tag{2}$$

(following an idea of [2]), which in turn may be diagonalized in terms of free fermions [3]. Note that H_{long} commutes with σ_0^x and σ_{L+1}^x. Hence the spectrum of H_{long} decomposes into four sectors $(+,+)$, $(+,-)$, $(-,-)$, $(-,+)$ corresponding to the eigenvalues ± 1 of σ_0^x and σ_{L+1}^x. The spectrum and the eigenvectors of H are obtained by projecting onto the $(+,+)$-sector.

In this paper we are going to consider the profiles of the spin operators σ_j^z and σ_j^x. We have already shown in [1] how to compute the one-point function of the σ_j^x-operator in terms of Pfaffians. The σ_j^z-profiles are easier to compute. We will study the ground-state profiles as well as the profiles of certain excited states of H. The excited states of H we are going to consider correspond to single fermion excitations with respect to the ground state of H_{long}, which are characterized by a non-vanishing excitation energy as L goes to infinity and which correspond to boundary bound states.

0305-4470/00/437661+26$30.00

We are able to obtain exact results for the ground-state profiles only for certain values of the boundary parameters [1]. In the case of the σ_j^z-profiles we will find exact expressions on the finite chain, in the continuum limit $L \gg 1$, $z = j/L$ fixed and in the limit $L \to \infty$, $j \gg 1$. The σ_j^x-profiles are given in terms of Pfaffians of $2j \times 2j$ matrices, that we have not been able to compute on the finite chain or in the continuum limit exactly, therefore our exact results for the σ_j^x-profiles are restricted to the limit $L \to \infty$, $j \gg 1$.

A combination of extensive numerical computations (for lattice lengths $L \sim 600$) and of our exact results has led us to conjectures for the profiles of σ_j^z and σ_j^x in the continuum limit for more general values of the boundary parameters. Note that once we know the σ_j^x-profile for one specific choice of the boundary terms, we know already the profile of σ_j^y for the boundary terms with σ^x and σ^y interchanged in (1).

We will discuss our results for the ground-state profiles in the context of conformal field theory. According to Burkhardt and Xue [4, 5], in the continuum limit $z = j/L$, $L \gg 1$ the general form of the profile of any scalar scaling operator ϕ with bulk-scaling dimension x_ϕ is given by

$$\langle \phi(j) \rangle_{ab} = [(L/\pi)\sin(\pi z)]^{-x_\phi} \mathcal{F}_{ab}(z). \tag{3}$$

The functional form of $\mathcal{F}_{ab}(z)$ depends on the boundary conditions a and b at the left and the right-hand boundary respectively. We have shown in [6] that the *XX*-model with Hermitian boundaries corresponds to the free compactified boson on a cylinder with Neumann–Neumann (NN), Dirichlet–Neumann (DN) or Dirichlet–Dirichlet (DD) boundary conditions. The bulk-scaling dimensions x_ϕ obtained from the two-point functions for the periodic chain are 1 ($\frac{1}{4}$) for σ_j^z (σ_j^x) [7, 8].

Conformal field theory makes more restrictive predictions for the behaviour of the profiles of scaling operators near the boundary. From (3) we obtain that near the boundary the profile is given by

$$\langle \phi(j) \rangle_{ab} = j^{-x_\phi} \psi_{ab}(z) \qquad z \ll 1. \tag{4}$$

It was already argued in [9] that if the scaling function $\psi_{ab}(z)$ is different from zero near the boundary it has the asymptotic form

$$\psi_{ab}(z) = A[1 + \mathcal{B}_{ab}^{\phi} z^2 + \cdots] \qquad z \ll 1. \tag{5}$$

Furthermore it has been shown in [4, 5, 10] that the amplitude $\mathcal{B}_{ab}^{\phi}$ is related to the Casimir amplitude $\mathcal{A}_{ab}$ via

$$\mathcal{B}_{ab}^{\phi}/\mathcal{A}_{ab} = -4\pi x_\phi / c \tag{6}$$

where c denotes the central charge of the theory. The Casimir amplitude $\mathcal{A}_{ab}$ is defined by the large-L behaviour of the ground-state energy E_0, i.e.

$$E_0 = e_\infty L + f_{ab} + \mathcal{A}_{ab} L^{-1} + \cdots \tag{7}$$

where by e_∞ and f_{ab} we denote the bulk and the surface free energy respectively. The Casimir amplitudes for the boundary terms of the Hamiltonian (1) can be read off from the partition functions obtained in [6, 11].

As we are going to show, when dealing with boundaries, it is not *a priori* clear which combinations of spin operators correspond to the scaling operators of the continuum theory. Our conjectures for the continuum limit of the profiles will yield that the profiles of σ_j^x and of σ_j^z indeed have the form of (3) (see however equation (35)).

We will see that if the boundary conditions we are going to consider correspond to DN of the free boson field the profiles satisfy (5) and (6). We will also see that for the boundary terms corresponding to DD and NN boundary conditions the profiles show a more complicated

behaviour near the boundary. In these cases the equations (5) and (6) do not hold in general for the profiles of σ_j^x and σ_j^z.

In the case of DD boundary conditions we have to build an appropriate linear combination of σ_j^z and σ_{j+1}^z in order to obtain the correct behaviour of a scaling operator. However, in the generic case the linear combination we are going to obtain works only at one boundary at a time. The σ_j^x-profile vanishes exactly in this case.

For the case of NN boundary conditions we obtain the correct behaviour by considering a linear combination of σ_j^x and σ_j^y. Again this works only at one boundary at a time in the generic case. Here the σ_j^z-profile vanishes if no diagonal boundary terms are present at the boundary (i.e. $\alpha_z = \beta_z = 0$). However, we have also studied a type of boundary corresponding to the NN boundary conditions, where diagonal and non-diagonal boundaries are present at a boundary at the same time. In this case the profile of the σ_j^z-operator vanishes only in the leading order and is determined by a secondary field instead of by a primary field.

Our results in the limit $L \to \infty$, $j \gg 1$ are in agreement with the results of Affleck [12]. He has considered the semi-infinite XXZ spin-$\frac{1}{2}$ chain with a transverse magnetic field applied at the end of the chain (this corresponds to $\alpha_+ = \alpha_- \neq 0$, $\alpha_z = \beta_z = \beta_+ = \beta_- = 0$ and $L \to \infty$ in our notation). Affleck has used the bosonization technique, whereas our results have been obtained on the lattice. Assuming Neumann boundary conditions for the boson field, he obtained the σ_j^x-profile for large values of j. At the free-fermion point the result reads

$$\langle \sigma_j^x \rangle = (-1)^j C j^{-\frac{1}{4}} \tag{8}$$

where the constant C does not depend on the strength of the field and at the free-fermion point its numerical value is given by

$$C = 0.912\,171\,210\,446\ldots. \tag{9}$$

The case of a longitudinal magnetic field at the end of the chain has also been considered in [12] (corresponding to $\alpha_z \neq 0$, $\alpha_+ = \alpha_- = \beta_z = \beta_+ = \beta_- = 0$ and $L \to \infty$). Imposing Dirichlet boundary conditions for the boson field, the large-j behaviour of the σ_j^z-profile has been evaluated for small values of α_z, yielding at the free-fermion point

$$\langle \sigma_j^z \rangle \approx B\alpha_z (-1)^j j^{-1} \tag{10}$$

where the value of B is undetermined. The case of diagonal and non-diagonal boundary terms at the boundary at the same time has not been considered. The boundary conditions where we have been able to compute the profiles exactly in the limit $L \to \infty$, $j \gg 1$ can always be mapped onto the boundaries treated by Affleck. Our results obtained on the lattice agree with (8) and (10). For the σ_j^z-profiles we have not restricted ourselves to small values of α_z and we have derived the α_z-dependence of B.

As already mentioned above, we will also consider the magnetization profiles of certain eigenstates of H, which are obtained by the excitation of a massive fermion with respect to the ground state of H_{long}. The existence of such fermions has already been mentioned in [1] for special values of the boundary parameters. Before considering the profiles, we are going to study the appearance of such fermions for general, Hermitian boundary terms.

We will see that massive fermions appear if the values of certain functions of the boundary parameters become greater than a certain threshold. The respective excitation masses will turn out to depend only on the boundary parameters of one boundary at a time. In the general case (non-diagonal together with diagonal boundary terms) we will find at most one mass per boundary.

In the case of purely diagonal boundary terms the fermion masses correspond exactly to the non-vanishing energy gaps obtained in the Bethe ansatz by comparing the energy of the

reference state with the energy of the one-magnon excitations, which correspond to boundary 1-strings [13].

We will see that the magnetization profiles for the excited states under study here show an exponential fall-off into the bulk for diagonal as well as for non-diagonal boundary conditions (the profiles for the non-diagonal boundary terms have been obtained numerically). Hence we are going to refer to these states as to boundary bound states. These profiles appear also for H since the excited states we are going to study lie in the (+, +)-sector of the Hilbert space of H_{long} and do therefore correspond directly to eigenstates of H.

This paper is organized as follows: we start with the exact results in section 2. These results are restricted to certain choices of boundary terms. In section 3 we will give our conjectures for the profiles in the continuum limit for more general types of boundary. We shall discuss these results in the context of conformal field theory in section 4. Boundary bound states are the subject of section 5. Our conclusions will be given in section 6. The details of our calculations will be given in the appendices. In appendix A we briefly discuss the diagonalization of H_{long} and the projection onto the (+, +)-sector in order to provide the basic facts and notations being necessary to follow our calculations. Appendix B deals with the exact computations of the σ_j^z-profiles. How we arrived at our exact results for the σ_j^x-profiles is shown in appendix C. In appendix D we discuss the numerical verification of our conjectures of the ground-state profiles in the continuum limit.

2. Exact results

For technical reasons explained in appendix A, we have been able to obtain analytical results only for certain choices of boundary terms (see tables 1 and 2). We will begin with the results for the σ_j^z-profiles on the finite chain, before turning to the respective expressions in the continuum limit. Thereafter we will give our exact results in the limit $L \to \infty$, $j \gg 1$ for the profiles of σ_j^x and σ_j^z.

2.1. Exact results on the finite lattice ($\langle\sigma_j^z\rangle$- profiles)

We have computed the exact profiles of σ_j^z for values of the boundary parameters given in table 1†. Note that for technical reasons (see appendix B for details) our result for case e is restricted to the choice $\delta = 0$ in this section. Furthermore, observe that the ground state is twofold degenerate for case d with L odd and for case e with L even, due to the existence of additional zero modes [1]. In these cases, we have obtained the profiles for the two ground states, which have a well defined fermion number (see appendix B). These profiles are indicated by a $\pm$-sign in the respective expressions.

Case a.

$$\langle\sigma_j^z\rangle = \frac{1}{2L+2}\left((-1)^L \tan\frac{\pi}{4L+4} + (-1)^j \cot\frac{(2j-1)\pi}{4L+4}\right). \tag{11}$$

Case b.

$$\langle\sigma_j^z\rangle = \frac{(-1)^j}{2L+1}\cot\frac{(2j-1)\pi}{4L+2}. \tag{12}$$

† The cases denoted by a, b, c, d, e correspond to the cases 2, 4, 11, 14, 16 in the notation of [1, 6].

Table 1. The values of the boundary parameters where we have computed the ground-state profiles of σ_j^z exactly on the finite chain and in the continuum limit. By DN and DD we denote the respective boundary conditions on the free boson [6]. For case e there appears a free, real parameter δ.

Case	α_z	β_z	$\beta_+ = \beta_-$	$\alpha_\pm$	
a	$\frac{1}{\sqrt{2}}$	0	$\frac{1}{\sqrt{2}}$	0	DN
b	$\frac{1}{\sqrt{2}}$	0	1	0	DN
c	$\frac{1}{\sqrt{2}}$	0	0	0	DD
d	$\frac{1}{\sqrt{2}}$	$\frac{-1}{\sqrt{2}}$	0	0	DD
e	$\frac{1}{\sqrt{2}}\tan\left(\frac{\pi}{4}+\frac{\delta}{2}\right)$	$\frac{1}{\sqrt{2}}\tan\left(\frac{\pi}{4}-\frac{\delta}{2}\right)$	0	0	DD

Case c.

$$\langle\sigma_j^z\rangle = \frac{1}{2L+1}\left((-1)^L + (-1)^j\left(\sin\frac{(2j-1)\pi}{4L+2}\right)^{-1}\right). \tag{13}$$

Case d. L odd: the ground state is twofold degenerate in this case.

$$\langle\sigma_j^z\rangle_\pm = \frac{1}{L}\left((-1)^j\cot\frac{(2j-1)\pi}{2L} \pm 1\right). \tag{14}$$

Case d. L even

$$\langle\sigma_j^z\rangle = \frac{(-1)^j}{L}\left(\sin\frac{(2j-1)\pi}{2L}\right)^{-1}. \tag{15}$$

Case e. L odd, $\delta = 0$: the same as given for case d, L even.

Case e. L even, $\delta = 0$: the same as given for case d, L odd. The ground state is twofold degenerate in this case, too.

2.2. Exact results in the continuum limit

The continuum limit of the expressions (11)–(15) defined by $L \gg 1$, $z = j/L$ fixed is readily obtained. Furthermore we have been able to compute the profile in the continuum limit for case e for general values of δ (see appendix B).

Cases a and b.

$$\langle\sigma_j^z\rangle = (-1)^j(L\sin(\pi z))^{-1}\cos^2\left(\frac{\pi z}{2}\right) + \mathrm{O}\left(\frac{1}{L^2}\right). \tag{16}$$

Case c.

$$\langle\sigma_j^z\rangle = (-1)^j(L\sin(\pi z))^{-1}\cos\left(\frac{\pi z}{2}\right) + \frac{(-1)^L}{2L} + \mathrm{O}\left(\frac{1}{L^2}\right). \tag{17}$$

Table 2. Boundary parameters for the cases where we found exact expressions for the ground-state profiles of σ_j^x in the limit $L \to \infty$, $j \gg 1$. The first case corresponds to DN boundary conditions, whereas the second case corresponds to NN boundary conditions on the free boson. The free parameters χ and φ are real constants.

Case	α_+	α_-	β_+	β_-	
f	1	1	0	0	DN
g	$e^{i\varphi}$	$e^{-i\varphi}$	$e^{i(\chi+\varphi)}$	$e^{-i(\chi+\varphi)}$	NN

Case d. The same expression as given for case e with $\delta = 0$ and L even and L odd interchanged.

Case e. L odd

$$\langle\sigma_j^z\rangle = (-1)^j \cos\delta (L \sin(\pi z))^{-1} + \mathrm{O}\left(\frac{1}{L^2}\right). \tag{18}$$

Case e. L even

$$\langle\sigma_j^z\rangle_\pm = (-1)^j \cos(\delta \mp \pi z)(L \sin(\pi z))^{-1} \pm 1/L + \mathrm{O}\left(\frac{1}{L^2}\right). \tag{19}$$

2.3. Exact results in the limit $L \to \infty$, $j \gg 1$

We have obtained exact results for the profiles of σ_j^z in the limit $L \to \infty$, $j \gg 1$ for the five cases given in table 1. For the cases a, b, c and d the result may be read of from the expressions obtained on the finite lattice. This cannot be done for case e with arbitrary values of δ, since the respective result on the finite lattice is restricted to $\delta = 0$. However, in the limit $L \to \infty$, $j \gg 1$ the calculation for case e can be performed for arbitrary values of δ (see appendix B). Using α_z instead of the parameter δ (see table 1 for the relation between δ and α_z) we have obtained

$$\langle\sigma_j^z\rangle = (-1)^j \frac{\sqrt{8}\alpha_z}{(1+2\alpha_z^2)\pi} j^{-1} + \cdots. \tag{20}$$

The profiles for the cases a, b, c and d are also given by this expression if one replaces α_z by $\frac{1}{\sqrt{2}}$. The result (20) has to be compared to (10), which yields B as a function of α_z, i.e.

$$B = \frac{\sqrt{8}}{(1+2\alpha_z^2)\pi}. \tag{21}$$

We have obtained exact results for the profiles of σ_j^x in the limit $L \to \infty$ and $j \gg 1$ for the two cases given in table 2†. Our computations for case f (see appendix C2) yield

$$\langle\sigma_j^x\rangle = (-1)^j A j^{-\frac{1}{4}} + \cdots \tag{22}$$

where A is given by

$$A = e^{1/4} 2^{7/12} C_G^{-3} \tag{23}$$

and C_G is Glaisher's constant [14], which can be approximately given by

$$C_G = 1.282\,427\,129\,100\,62\ldots. \tag{24}$$

† In the notation of [1, 6] these cases correspond to case 2 and case 9 respectively.

For case g we have obtained (see appendix C1)

$$\langle\sigma_j^x\rangle = (-1)^j A\cos\varphi j^{-\frac{1}{4}} + \cdots. \tag{25}$$

Comparing the value of C in (9) and the value of A in (23) using (24) shows that our results (22) and (25) for $\varphi = 0$ are in agreement with (8).

At this point we want to draw the reader's attention to an interesting by-product we have obtained during our computations for case g. It is of major interest for our conjecture of the continuum limit of the σ_j^x profiles in the case of NN boundary conditions presented in the next section. We have obtained that the ground-state profile of σ_j^x for arbitrary values of φ and χ (see table 2) is given by

$$\langle\sigma_j^x\rangle = \cos\left(\varphi + \frac{\chi + 2m\pi}{L+1}j\right) f(j, L) \tag{26}$$

where $f(j, L)$ does not depend on φ, χ and may be computed numerically (see appendix C1). The value of m depends on the value of χ and on the lattice length L. For odd L we have $m = 0$ for $-\pi < \chi < \pi$. If $\chi = \pi$ the ground state of H is twofold degenerate. The value of m is either 0 or -1. For even L the value of m is $\frac{1}{2}$ for $0 > \chi > -\pi$ and $-\frac{1}{2}$ for $0 < \chi \leqslant \pi$. Here the ground state is twofold degenerate for $\chi = 0$, the value of m being either $\frac{1}{2}$ or $-\frac{1}{2}$.

3. Conjectures

Our results given so far allow us to conjecture the ground-state profiles in the continuum limit for more general values of the boundary parameters. We have checked our results by computing the profiles on the finite chain numerically for lattice lengths up to $L = 700$. Thereafter we have used the finite-size data to extrapolate the profiles for $L \to \infty$ and fixed values of $z = j/L$. We have performed these extrapolations for 150 different values of the boundary parameters each with 19 (L even) or 20 (L odd) values of z. The accuracy of our extrapolations varies with the choice of the boundary parameters. In most of the cases the relative deviation from our conjectures presented in the following has been of the order of 10^{-12}–10^{-7} (see appendix D for details).

We have considered the following types of boundary term.

- DD:

$$\alpha_\pm = \beta_\pm = 0 \qquad \alpha_z = \frac{1}{\sqrt{2}}\tan\left(\frac{\omega+\delta}{2}\right) \qquad \beta_z = \frac{1}{\sqrt{2}}\tan\left(\frac{\omega-\delta}{2}\right). \tag{27}$$

  Note that for $\omega = \frac{\pi}{2}$ we recover the boundary terms of case e in table 1.
- DN: here we have considered only a special type of boundary term, i.e.

$$\beta_+ = \beta_- \neq 0 \qquad \beta_z = \alpha_\pm = 0 \qquad \alpha_z \text{ free.} \tag{28}$$

- NN: we have studied two types of boundary term, i.e.

$$\alpha_z = \beta_z = 0 \qquad \alpha_\pm = R_\alpha \mathrm{e}^{\pm \mathrm{i}\varphi} \qquad \beta_\pm = R_\beta \mathrm{e}^{\pm \mathrm{i}(\chi+\varphi)} \tag{29}$$

  and

$$\alpha_z = -\beta_z \qquad \alpha_+ = \alpha_- = \beta_+ = \beta_- \neq 0. \tag{30}$$

Note that the boundary terms (29) are identical to the boundaries of case g in table 2 if one sets $R_\alpha = R_\beta = 1$, whereas no case in tables 1 and 2 corresponds to boundary terms which satisfy (30). In this case our result is based on purely numerical computations. Observe, also, that this is the only type of boundary term with diagonal and non-diagonal terms at one end of the chain, which is studied in this paper.

Table 3. Dependence of Q on ω and L.

	$-\pi < \omega < -\frac{\pi}{2}$	$-\frac{\pi}{2} < \omega < 0$	$0 < \omega < \frac{\pi}{2}$	$\frac{\pi}{2} < \omega < \pi$
L even	$Q = 1$	$Q = 0$	$Q = 0$	$Q = -1$
L odd	$Q = \frac{1}{2}$	$Q = \frac{1}{2}$	$Q = -\frac{1}{2}$	$Q = -\frac{1}{2}$

3.1. DD boundary conditions

For this type of boundary condition the ground-state profile of σ_j^x vanishes if the ground state is non-degenerate, since the Hamiltonian commutes with $\sigma_1^z \sigma_2^z \dots \sigma_L^z$. Therefore we have restricted ourselves to the ground-state profiles of σ_j^z. Our results for the cases c, d and e from table 1 and our numerical investigations suggest the σ_j^z-profiles for general values of α_z and β_z, i.e.

$$\langle \sigma_j^z \rangle = (-1)^j \frac{\sin(\omega + \delta - 2(\omega + Q\pi)z)}{L \sin(\pi z)} + \frac{2(\omega + Q\pi)}{\pi L}. \tag{31}$$

This equation is valid for L even and odd. The value of Q depends on the values of ω and the lattice length L. This dependence is given in table 3. The discontinuities are due to level crossings in the spectrum at the respective values of ω. At these points ($\omega = 0$ for L odd and $\omega = \pm\pi/2$ for L even) the ground state is twofold degenerate.

3.2. DN boundary conditions

Our numerical computations suggest the following profile of the σ_j^x-operator:

$$\langle \sigma_j^x \rangle = \pi^{1/4} A (-1)^{L+1-j} \left[\sin\left(\frac{\pi z}{2}\right) \right]^{\frac{1}{2}} (L \sin(\pi z))^{-\frac{1}{4}} \tag{32}$$

where A is given by (23).

For two cases corresponding to this type of boundary we have already considered the exact σ_j^z-profiles, namely for case a and b from table 1. The given expression (16) suggests universal behaviour with respect to the variation of the value of $\beta_\pm$. Our numerical calculations for various values of $\beta_\pm$ confirmed our guess. Furthermore they yield the dependence of the profile on the second parameter α_z. We have obtained

$$\langle \sigma_j^z \rangle = (-1)^j \frac{\sqrt{8}\alpha_z}{1 + 2\alpha_z^2} \cos^2\left(\frac{\pi z}{2}\right) (L \sin(\pi z))^{-1}. \tag{33}$$

Note that the form of the profile does not depend on the value of α_z. However, observe also that the amplitude does. For $\alpha_z = 0$ the profile vanishes, since then the Hamiltonian H commutes with $\sigma_1^x \sigma_2^x \dots \sigma_L^x$ (the ground state of H is non-degenerate [1]).

3.3. NN boundary conditions

Our exact result for case g from table 2, in particular equation (26), in combination with numerical computations yields the σ_j^x-profile for the first type of boundary in question (see (29)):

$$\langle \sigma_j^x \rangle = \pi^{1/4} A (-1)^j \cos(\varphi + (\chi + 2m\pi)z)(L \sin(\pi z))^{-\frac{1}{4}} \tag{34}$$

where the value of m depends on the values of χ and the lattice length L as already discussed at the end of section 2.3. The σ_j^z profiles vanish, as long as the ground state is non-degenerate

(see appendix B for details). We did not consider the σ_j^z profiles where the ground state is degenerate.

For the second type of boundary term (30) the σ_j^z profile does not vanish. For odd values of L our numerical investigations suggest

$$\langle\sigma_j^z\rangle = (-1)^j \pi\sqrt{2}\frac{\alpha_z}{\alpha_+^2}\cos(\pi z)(L\sin(\pi z))^{-2}. \tag{35}$$

We have not been able to find an analytic expression for the profile for even values of L. For $\alpha_+ = 0$ the prefactor in (35) diverges. However, in this case the profile is already given by (31). For $\alpha_z = 0$ the profile vanishes as in the case of the DN boundary condition (28), since in this case the Hamiltonian H has a higher symmetry. It commutes with $\sigma_1^x\sigma_2^x\ldots\sigma_L^x$ (the ground state of H is also non-degenerate here [1]).

Comparing (35) with (3) yields that the leading term of the σ_j^z-profile is zero as for the boundary terms (29), since according to the long-range behaviour of the two-point function the bulk-scaling dimension x_ϕ associated with the σ_j^z operator is 1. Since there exists no spinless primary field with bulk-scaling dimension 2 [15] we conclude that the profile (35) is determined by a secondary field (the profile of a primary field with spin vanishes [5]).

We have checked the σ_j^x-profile only for odd L. It is not affected by the presence of the diagonal terms in (30) and is already given by (34) using $\varphi = \chi = m = 0$.

4. Comparison with the predictions of conformal field theory

In this section we are going to consider the behaviour of the profiles we have conjectured near the boundaries, i.e. we consider the limit $z \ll 1$ (respectively $(1-z) \ll 1$), in order to check for the validity of the equations (5) and (6).

4.1. DD boundary conditions

The behaviour of (31) near the left-hand boundary is readily obtained:

$$\langle\sigma_j^z\rangle = (-1)^j\frac{\sin(\omega+\delta)}{j\pi}\left(1-\cot(\omega+\delta)2\omega' z+\left(\frac{1}{6}-\frac{2\omega'^2}{\pi^2}\right)(\pi z)^2+\cdots\right)+\frac{2\omega'}{\pi L} \tag{36}$$

where $\omega' = \omega + Q\pi$. The behaviour of the profile near the right-hand boundary may be obtained by exchanging δ for $-\delta$ and performing the transformation $j \mapsto L+1-j$. This can be seen from (27). Note that (36) does not agree with equation (5), since in (5) there appears no term which is linear in z. This problem is avoided by considering the profile of the following linear combination of σ_j^z and σ_{j+1}^z for odd values of j:

$$\left\langle\tan\left(\frac{\omega+\delta}{2}\right)\sigma_j^z-\cot\left(\frac{\omega+\delta}{2}\right)\sigma_{j+1}^z\right\rangle = -\frac{2}{j\pi}\left(1+\left(\frac{1}{6}-\frac{2\omega'^2}{\pi^2}\right)(\pi z)^2+\cdots\right). \tag{37}$$

The value of the Casimir amplitude $\mathcal{A}_{ab}$ can be obtained from the results in [6, 11]. It is given by $\mathcal{A}_{ab} = -\frac{\pi}{24}+\frac{\omega'^2}{2\pi^2}$. Hence (37) is in agreement with (6). Note that this operator does not yield the correct scaling behaviour near the right-hand boundary, since the given linear combination of σ_j^z and σ_{j+1}^z depends on the value of δ, which enters the left-hand boundary term in a different way than the right-hand boundary term (see (27)). Another linear combination can be chosen to obtain the correct behaviour near the right-hand boundary.

4.2. DN boundary conditions

The Casimir amplitude for this type of boundary condition is independent from the explicit values of the boundary parameters. Its value is given by $\mathcal{A}_{ab} = \frac{\pi}{48}$ [6]. The profiles (32)

and (33) vanish near the left- and near the right-hand boundary respectively and therefore the predictions (5) and (6) are not valid. Near the right-hand boundary we obtain from (32)

$$\langle \sigma^x_{L+1-j} \rangle = (-1)^j A j^{-\frac{1}{4}} \left(1 - \frac{(\pi z)^2}{48} + \cdots \right) \tag{38}$$

whereas (33) yields near the left-hand boundary

$$\langle \sigma^z_j \rangle = (-1)^j \frac{\sqrt{8}\alpha_z}{1+2\alpha_z^2} (j\pi)^{-1} \left(1 - \frac{(\pi z)^2}{12} + \cdots \right). \tag{39}$$

Both expressions are in agreement with the predictions (5) and (6).

4.3. NN boundary conditions

From (34) we obtain the profiles of σ^x_j near the left-hand boundary, i.e.

$$\langle \sigma^x_j \rangle = (-1)^j A j^{-\frac{1}{4}} \cos\varphi \left(1 - \tan(\varphi)(\chi + 2m\pi) z + \left(\frac{\pi^2}{24} - \frac{(\chi + 2m\pi)^2}{2} \right) z^2 + \cdots \right). \tag{40}$$

The Casimir amplitude has been shown in [6] to be $\mathcal{A}_{ab} = -\frac{\pi}{24} + 2\pi(m + \frac{\chi}{2\pi})^2$. Note that the profile is in disagreement with the predicted behaviour for a true scaling operator given in (5). In order to obtain the correct behaviour near the boundary, we have to consider an appropriate linear combination of σ^x_j and σ^y_j. At the left-hand boundary we obtain

$$\langle \cos\varphi \sigma^x_j - \sin\varphi \sigma^y_j \rangle = (-1)^j A j^{-\frac{1}{4}} \left(1 + \left(\frac{\pi^2}{24} - \frac{(\chi + 2m\pi)^2}{2} \right) z^2 + \cdots \right) \tag{41}$$

which is in agreement with (5) and (6). Note that building the given linear combination is equivalent to performing a rotation around the z-axis such that $\varphi = 0$ in (29). However, similar to the case of the σ^z_j profile for the DD boundary condition, this linear combination does not lead to the correct behaviour near the right-hand boundary. To obtain the correct behaviour near the right-hand boundary one has to perform a different rotation as long as $\chi \neq 0$.

It is interesting to consider the respective profile of the orthogonal linear combination of σ^x_j and σ^y_j, which yields

$$\langle \sin\varphi \sigma^x_j + \cos\varphi \sigma^y_j \rangle = -(-1)^j A j^{-\frac{1}{4}} ((\chi + 2m\pi) z + \cdots). \tag{42}$$

Note that this profile vanishes near the left-hand boundary and therefore the predictions (5) and (6) do not apply.

5. Boundary bound states

As already mentioned in the introduction, we have also studied the profiles of certain excited states of H. These states are obtained by the excitation of a massive fermion with respect to the ground state of H_{long}. We refer to these excitations as boundary excitations, since we are going to see that they give rise to a contribution to the profile which decays exponentially into the bulk.

First, we are going to look for massive excitations for general, Hermitian boundary terms in section 5.1 by studying the secular equation $p(x^2) = 0$ which determines the fermion energies and which has been obtained in [1]. In section 5.2 we will study the magnetization profiles near the boundaries of the states, where one massive fermion is excited, for two special types of boundary term.

In the case of diagonal boundary terms the energy gaps defined with respect to the ground-state energy are in one to one correspondence to the boundary 1-strings found as solutions of the Bethe ansatz equations. The 1-strings define the energy gaps between the energy of the reference state and the eigenstates in the one-magnon sector. At the free-fermion point a boundary 1-string appears if $2\alpha_z^2$ or $2\beta_z^2 > 1$ [13]. The energy gaps corresponding to the boundary 1-strings in the limit $L \to \infty$ are given by

$$E_\alpha = \frac{1}{2}\left(\frac{1}{\sqrt{2}\alpha_z} + \sqrt{2}\alpha_z\right) \qquad E_\beta = \frac{1}{2}\left(\frac{1}{\sqrt{2}\beta_z} + \sqrt{2}\beta_z\right) \tag{43}$$

where by E_α and E_β we denote the energy gaps corresponding to the boundary 1-string which appears for $2\alpha_z^2 > 1$ and $2\beta_z^2 > 1$ respectively.

5.1. Massive excitations

The fermion energies are obtained by

$$2\Lambda = \frac{1}{2}\left(x + \frac{1}{x}\right) \tag{44}$$

where the values of x are given by the roots of a polynomial $p(x^2)$ [1]. Since the energies have to be real numbers, the roots of the polynomial lie either on the unit circle or on the real axis. We will focus on the roots which lie on the real axis for $L \to \infty$. Due to (44) these roots yield fermions with a finite energy in this limit. We have not been able to determine whether there exist massive fermions corresponding to roots lying on the unit circle.

We are going to restrict ourselves to the search for zeros satisfying $|x| < 1$, since if x is a zero of $p(x^2)$ so is $1/x$. In the limit $L \to \infty$, the secular equation $p(x^2) = 0$ reduces to

$$(1 + (1 - 2\alpha_z^2 - 2\alpha_-\alpha_+)x^2 - 2\alpha_z^2x^4)(1 + (1 - 2\beta_z^2 - 2\beta_-\beta_+)x^2 - 2\beta_z^2x^4) = 0. \tag{45}$$

Solving for x^2 yields two solutions with $|x^2| < 1$, i.e.

$$x^2 = \frac{1}{4\alpha_z^2}\left[1 - 2\alpha_-\alpha_+ - 2\alpha_z^2 + \sqrt{8\alpha_z^2 + (2\alpha_z^2 + 2\alpha_-\alpha_+ - 1)^2}\right] \tag{46}$$

and

$$x^2 = \frac{1}{4\beta_z^2}\left[1 - 2\beta_-\beta_+ - 2\beta_z^2 + \sqrt{8\beta_z^2 + (2\beta_z^2 + 2\beta_-\beta_+ - 1)^2}\right]. \tag{47}$$

Note that these solutions depend only on the parameters of one boundary at a time. The fermion energies are obtained by taking the positive square root of (46) respectively (47) and using (44). Hence we conclude that the maximum number of massive excitations obtained by our ansatz is two (one per boundary). This result is interesting since it confirms an analogous result obtained by Ameduri *et al* [16] in their study of the boundary sine–Gordon theory at the free-fermion point.

If the value of α_z or β_z is equal to zero, the expression (46) or (47) respectively has to be replaced by

$$x^2 = 1/(2\alpha_-\alpha_+ - 1) \qquad \text{respectively} \quad x^2 = 1/(2\beta_-\beta_+ - 1). \tag{48}$$

If α_- or $\alpha_+ = 0$ (β_- or $\beta_+ = 0$) the result simplifies to

$$x^2 = 1/(2\alpha_z^2) \qquad \text{respectively} \quad x^2 = 1/(2\beta_z^2). \tag{49}$$

All solutions of (45) are only asymptotic solutions of the original polynomial if they satisfy the assumption $|x| < 1$. In the case of diagonal boundary terms this condition coincides with the condition for the existence of boundary 1-strings in the Bethe ansatz. The energies of the one-magnon excitations corresponding to the boundary 1-strings given in (43) correspond exactly to the fermion energies (44) obtained by the roots in (49).

5.2. Magnetization profiles near the boundary

We have studied the magnetization profiles for certain states, which differ from the ground state of H_{long} by a boundary excitation, for two types of boundary. Note that the ground state of H_{long} is at least twofold degenerate. We have chosen it such that the excited state in question lies in the $(+,+)$-sector. Therefore these states correspond also to eigenstates of H. First we have considered diagonal boundary terms

$$\alpha_z = 1/(2\beta_z) = \mathrm{e}^{\xi}/\sqrt{2} \qquad \alpha_\pm = \beta_\pm = 0 \tag{50}$$

for even and odd values of L. Without loss of generality we have restricted ourselves to $\xi > 0$. In this case $2\alpha_z^2$ becomes larger than unity and according to (49) and (44) there exists one boundary excitation with energy $2\Lambda = \cosh\xi$. We are able to compute the σ_j^z-profile analytically in the limit $L \to \infty$, $j \gg 1$ (see appendix B), i.e.

$$\langle\xi|\sigma_j^z|\xi\rangle \approx \frac{(-1)^j}{\pi}\frac{1}{\cosh\xi}\,j^{-1} + 2(\mathrm{e}^{2\xi} - 1)\mathrm{e}^{-2j\xi} \tag{51}$$

where $|\xi\rangle$ denotes the state obtained by the excitation of the massive fermion. Observe that the correlation length $1/(2\xi)$ is related to the excitation mass $2\Lambda = \cosh\xi$. The profile near the right-hand boundary is

$$\langle\xi|\sigma_{L+1-j}^z|\xi\rangle \approx \frac{(-1)^j}{\pi}\frac{1}{\cosh\xi}\,j^{-1} \tag{52}$$

as expected. The $U(1)$-charge, which is given by the projection of the total spin onto the z-axis, of the state $|\xi\rangle$ is 0 for L even and $\frac{1}{2}$ for L odd.

Notice that the exponential part in (51) is not present if one considers the respective ground-state profile (see (20)). We conclude that adding a massive excitation to the ground state yields an additive contribution to the profile which decays exponentially into the bulk.

The second type of boundary we have considered are non-diagonal and given by

$$\alpha_\pm = \sqrt{\cosh\xi_\alpha \exp\xi_\alpha} \qquad \beta_\pm = \sqrt{\cosh\xi_\beta \exp\xi_\beta} \quad \alpha_z = \beta_z = 0. \tag{53}$$

We restricted ourselves to even values of L, since in this case for odd values of L the excitation of a fermion with respect to the ground state of H_{long} does not lead to a state which lies in the $(+,+)$-sector and hence does not correspond to an eigenstate of H (see appendix C3 for details). Since the σ_j^z-profile vanishes exactly for the boundaries (53), we have studied the σ_j^x-profile in this case. In contrast to the σ_j^z-profiles given in (51) and (52) our results for the σ_j^x-profiles we are going to present are based on numerical computations for $L = \infty$ in the special case $\xi_\beta = -\xi_\alpha$ and for $L = 800$ in the general case.

In [1] we have shown that the σ_j^x-profiles for the boundaries given in (53) may be computed in terms of determinants of $j \times j$ matrices. In the case $\xi_\beta = -\xi_\alpha$ it is possible to compute these matrices analytically in the limit $L \to \infty$ (see appendix C3). Thus the numerical study of the profile near the boundaries is easier than in the general case. Here one boundary excitation appears with energy $2\Lambda = \cosh\xi_\alpha$ (see (48) and (44)). For $\xi_\alpha > 0$ we have obtained by numerical extrapolation from data for $j = 1, \ldots, 100$

$$\langle\xi_\alpha|\sigma_j^x|\xi_\alpha\rangle \approx (-1)^{j+1}Aj^{-\frac{1}{4}}(1 - 2\mathrm{e}^{(-1)^j\xi_\alpha}\mathrm{e}^{-2j\xi_\alpha}) \tag{54}$$

and

$$\langle\xi_\alpha|\sigma_{L+1-j}^x|\xi_\alpha\rangle \approx (-1)^j Aj^{-\frac{1}{4}} \tag{55}$$

where A is given by (23) and $|\xi_\alpha\rangle$ denotes the state obtained by the excitation of the fermion with energy $2\Lambda = \cosh\xi_\alpha$. Again the exponential term is absent from the respective expressions

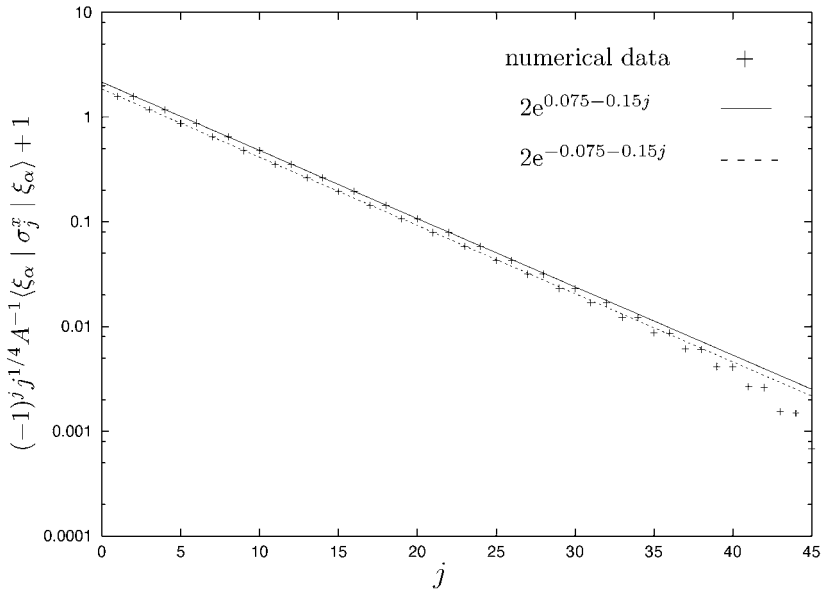

Figure 1. The exponential part of the σ_j^x-profile of the state $|\xi_\alpha\rangle$ near the left-hand boundary for the choice $\xi_\alpha = 0.075$, $\xi_\beta = 0.05$ in (53). The numerical data (+) have been obtained for $L = 800$. The two lines show the behaviour according to (54) for even respectively odd values of j. The deviation of the numerical data from the straight lines for large values of j is an effect of the finite lattice.

for the ground-state profile. Note again the relation between the correlation length and the excitation mass.

Inspired by this result we have also studied the case $\xi_\alpha \neq -\xi_\beta$. If $\xi_\alpha, \xi_\beta > 0$ there exist two boundary excitations with energies $2\Lambda_\alpha = \cosh \xi_\alpha$ and $2\Lambda_\beta = \cosh \xi_\beta$ in the limit $L \to \infty$. We have considered the respective magnetization profiles on the finite chain numerically ($L = 800$). Exemplarily the figures 1 and 2 show the profiles we have obtained numerically for the state $|\xi_\alpha\rangle$ near the left-hand and the right-hand boundary, where we have chosen $\xi_\alpha = 0.075$, $\xi_\beta = 0.05$.

Our results suggest that as long as $\xi_\alpha \neq \xi_\beta$ the profile for the state $|\xi_\alpha\rangle$ is still given by (54) and (55) (the deviation from the expression in (54) for large j in figure 1 is expected due to the presence of the right-hand boundary). The profile for the state $|\xi_\beta\rangle$ (obtained by the excitation of the fermion with energy $2\Lambda_\beta = \cosh \xi_\beta$) near the left-hand boundary is just

$$\langle \xi_\beta | \sigma_j^x | \xi_\beta \rangle \approx (-1)^j A j^{-\frac{1}{4}} \tag{56}$$

whereas at the right-hand boundary we have

$$\langle \xi_\beta | \sigma_{L+j-1}^x | \xi_\beta \rangle \approx (-1)^{j+1} A j^{-\frac{1}{4}} (1 - 2e^{(-1)^j \xi_\beta} e^{-2j\xi_\beta}). \tag{57}$$

However, if $\xi_\alpha = \xi_\beta = \xi$ our computations suggest a different behaviour, i.e.

$$\langle \xi_\alpha | \sigma_j^x | \xi_\alpha \rangle = \langle \xi_\beta | \sigma_j^x | \xi_\beta \rangle \approx (-1)^j A j^{-\frac{1}{4}} e^{(-1)^j \xi} e^{-2j\xi} \tag{58}$$

near the left-hand boundary and

$$\langle \xi_\alpha | \sigma_{L+1-j}^x | \xi_\alpha \rangle = \langle \xi_\beta | \sigma_{L+1-j}^x | \xi_\beta \rangle \approx (-1)^j A j^{-\frac{1}{4}} e^{(-1)^j \xi} e^{-2j\xi} \tag{59}$$

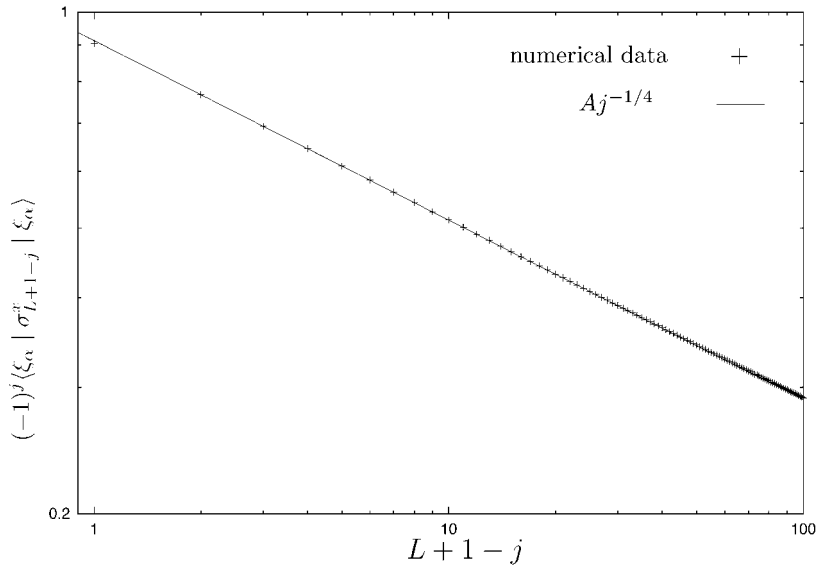

Figure 2. The σ^x_j-profile of the state $|\xi_\alpha\rangle$ near the right-hand boundary for the choice $\xi_\alpha = 0.075, \xi_\beta = 0.05$ in (53). The numerical data (+) have been obtained for $L = 800$. The straight line shows the behaviour according to (55).

near the right-hand boundary. In contrast to the profiles we have obtained so far, these profiles are left–right symmetric. Furthermore the leading term proportional to $j^{-\frac{1}{4}}$ does not appear, unlike the case in equations (54) and (57).

Note that the Hamiltonian with boundary conditions (53) conserves parity if $\xi_\alpha = \xi_\beta$. Our numerical computations yield that the energies $2\Lambda_\alpha$ and $2\Lambda_\beta$ are non-degenerate on the finite chain. Only in the limit $L \to \infty$ does the degeneracy appear. Hence the parity of the states $|\xi_\alpha\rangle$ and $|\xi_\beta\rangle$ is well defined. This explains why the profiles reflect the symmetry of the Hamiltonian.

6. Conclusions

In this paper we have studied the one-point functions of the σ^z_j and σ^x_j operator for the *XX*-chain with Hermitian boundaries, which in the continuum limit corresponds to a free boson field on a cylinder with DD, DN or NN boundary conditions [6].

No results for the magnetization profiles in the ground state have previously been obtained on the lattice. The only known results have been found by means of the bosonization technique [12] and were restricted to the limit $L \to \infty$ and $j \gg 1$ (see (8) and (10)). The expression (10) is valid only for small values of the longitudinal boundary field, i.e. for small values of α_z in our notation.

We have obtained the exact ground-state profiles of the σ^z_j-operator on the finite chain for the boundary terms given in table 1. The respective profiles are given in (11)–(15). The continuum limit of the profiles is given in (16)–(19).

The σ^z_j-profiles for the cases from table 1 in the limit $L \to \infty$, $j \gg 1$ are given in (20). Exact results for the σ^x_j-profiles in this limit have been found for the cases in table 2 and are given in (22) and (25) respectively. Our results obtained on the lattice agree with the

expressions (8) and (10) which have been found using the bosonization technique [12]. Note that in contrast to (10) our result (20) is not restricted to small values of the boundary field.

Supported by numerical computations, these exact results have led us to conjectures for the profiles in the continuum limit for more general values of the boundary parameters (see (27)–(30)). For the DD case we have studied the most general boundary terms (27). The σ_j^z-profile for these boundary terms is given in (31) (the σ_j^x-profile vanishes exactly if the ground state is non-degenerate).

We also considered a type of boundary term which corresponds to the DN boundary condition (see (28)). The σ_j^x-profile we conjectured is given in (32). The profile of the σ_j^z-operator is given in (33).

The boundary terms given by (29) and (30) correspond to NN boundary conditions on the boson field. The σ_j^x-profile for the first type of boundary (29) is given in (34). Here the σ_j^z-profile vanishes exactly, if the ground state is non-degenerate. For the second type of boundary term (30) the profile of the σ_j^z-operator is given in (35). As in the case of the DN boundary condition the σ_j^x-profile is not affected by the presence of the diagonal boundary terms.

The expressions we have obtained for the profiles in the case of the DD and the NN boundary conditions do not coincide with the predictions (5) and (6) conformal field theory makes for the profiles of scaling operators near a boundary. Here one has to consider certain linear combinations of spin-operators to obtain the correct behaviour. These combinations and the respective behaviour near the boundary are given in (37) and (40).

In this paper we have also discussed the appearance of massive excitations, i.e. of fermions with a non-vanishing energy as L goes to infinity. Such a fermion appears if the reciprocal value of one of the expressions (46) or (47) becomes larger than one. These expressions reduce to (48) respectively (49) in the case of purely non-diagonal respectively diagonal boundary terms.

We have computed the profiles near the boundaries in the limit $L \to \infty$, $j \gg 1$ for certain states with differ from the ground state of H_{long} by a massive excitation for boundary parameters satisfying (50) or (53). For the first type of boundary term there exists one massive excitation, whereas for the second type there might appear two of them. The profiles near the boundaries are given by (51) and (52) and by (54)–(57) respectively. If the value of ξ_α is equal to ξ_β (see (53)) the profiles are given by (58) and (59).

Acknowledgment

The author is grateful to V Rittenberg for many discussions and useful suggestions.

Appendix A. Diagonalization of H_{long} and the projection mechanism

In this appendix we are going to recapitulate the method we used in [1] to diagonalize H_{long} given in (2) and the projection mechanism, which yields the eigenvalues and eigenvectors of the Hamiltonian H in (1). This is necessary in order to fix the notation we are going to use during our computations for the profiles of σ_j^z and σ_j^x which are presented in appendix B and in appendix C respectively.

In its diagonal form H_{long} reads

$$H_{\text{long}} = \sum_{k=0}^{L+1} 2\Lambda_k b_k a_k - \sum_{k=0}^{L+1} \Lambda_k \tag{A.1}$$

where the b_k and a_k satisfy the anti-commutation relations of fermionic creation and annihilation operators. The factor 2 in equation (A.1) is just a remnant of our notation introduced in [1]. The values of the Λ_k are determined by the eigenvalues of a skew-symmetric $(2L+4) \times (2L+4)$ matrix M, i.e.

$$M(\phi_k^{\pm}) = \pm\Lambda_k(\phi_k^{\pm}). \tag{A.2}$$

The explicit form of M is given in [1]. The eigenvalues Λ_k can be obtained by the zeros x_k of a polynomial $p(x^2)$, which has also been given in [1], i.e.

$$\Lambda_k = \frac{1}{4}\left(x_k + \frac{1}{x_k}\right). \tag{A.3}$$

We have also shown in [1] how to compute the eigenvectors $(\phi_k^{\pm})$ as a function of the x_k and the boundary parameters $\alpha_{\pm}$, $\beta_{\pm}$, α_z and β_z. For certain choices of the boundary terms the x_k and the $(\phi_k^{\pm})$ can be computed exactly on the finite chain, since the polynomial $p(x^2)$ factorizes into cyclotomic polynomials [1]. For the boundary parameters given in tables 1 and 2 this is the case†. Otherwise the x_k and the $(\phi_k^{\pm})$ may be computed solving (A.2) numerically.

The eigenvectors $(\phi_k^{\pm})$ can be used to express the Clifford operators $\tau_j^{\pm}$, which are defined by

$$\tau_j^{+,-} = \left(\prod_{i=0}^{j-1}\sigma_i^z\right)\sigma_j^{x,y} \tag{A.4}$$

in the terms of the creation and annihilation operators b_k and a_k, i.e.

$$\tau_j^{\mu} = \sum_{k=0}^{L+1}(\phi_k^{-})_j^{\mu}a_k + (\phi_k^{+})_j^{\mu}b_k \tag{A.5}$$

where the $(\phi_k^{\pm})$ satisfy the orthogonality relation $\sum_{j,\mu}(\phi_l^{+})_j^{\mu}(\phi_k^{-})_j^{\mu} = \delta_{lk}$. Equation (A.5) allows us to write the spin operators in terms of the b_k, a_k and the eigenvectors $(\phi_k^{\pm})$. Therefore the knowledge of these vectors is a crucial point in view of the computation of the magnetization profiles. The vacuum state is defined by

$$a_k|\text{vac}\rangle = 0 \qquad \forall k. \tag{A.6}$$

Note that the vacuum state itself is not an element of one of the four sectors $(+,+)$, $(+,-)$, $(-,-)$ or $(-,+)$. However, in view of applications to the Hamiltonian H we are interested in the eigenstates of H_{long} which lie in the $(+,+)$-sector. Hence we have defined the states

$$|v^{\pm}\rangle = \frac{1}{\sqrt{2}}(1 \pm b_0)|\text{vac}\rangle \tag{A.7}$$

where b_0 denotes the creation operator of the spurious zero mode [1] which is always present in the spectrum of H_{long}. The associated eigenvectors $(\phi_0^{\pm})$ are given by

$$\phi_0^{+} = \left(0, \frac{1}{2}, 0, \ldots, 0, \frac{\mathrm{i}}{2}, 0\right) \qquad \phi_0^{-} = \left(0, \frac{1}{2}, 0, \ldots, 0, -\frac{\mathrm{i}}{2}, 0\right) \tag{A.8}$$

where we used the notation $(\phi_k^{\pm}) = ((\phi_k^{\pm})_0^{-}, (\phi_k^{\pm})_0^{+}, (\phi_k^{\pm})_1^{-}, (\phi_k^{\pm})_1^{+}, \ldots, (\phi_k^{\pm})_{L+1}^{-}, (\phi_k^{\pm})_{L+1}^{+})$. The states $|v^{\pm}\rangle$ satisfy

$$\sigma_0^x|v^{\pm}\rangle = \pm|v^{\pm}\rangle \qquad \sigma_{L+1}^x = \pm\eta|v^{\pm}\rangle \tag{A.9}$$

where $\eta^2 = 1$. If $\eta = 1$ the state $|v^{+}\rangle$ is an element of the $(+,+)$-sector and so are all the states obtained by an even number of fermion excitations, where we disregard the spurious

† They correspond to the factorizable cases 2, 4, 9, 11, 14 and 16 in the notation of [1].

zero mode. If $\eta = -1$ all the states obtained by the excitation of an odd number of fermions with respect to the state $|v^-\rangle$ are elements of the (+, +)-sector and hence build up the spectrum of H, where we again have to disregard the spurious zero mode. In the case of Hermitian boundaries the value of η may be computed via [1]

$$\eta = (-1)^{L+1} \frac{\alpha_- \beta_+ + \alpha_+ \beta_-}{4^{L+1} \prod_{k \neq 0} \Lambda_k}. \tag{A.10}$$

Note that (A.10) is of no use if there exist additional zero modes on top of the spurious zero mode.

Appendix B. Calculation of the σ_j^z-profiles

In this appendix we are going to explain how to compute the σ_j^z-profiles and how we have derived the ground-state profiles for the boundary terms in table 1, i.e. equations (11)–(20). We will also derive the profiles (51) and (52) associated with the excitation of the massive fermion appearing for the boundaries (50). Note that these boundaries coincide with the boundary terms of case e in table 1 if one identifies e^{ξ} with $\tan(\frac{\pi}{4} + \frac{\delta}{2})$.

Using (A.5), (A.7) and (A.8) one can show that the σ_j^z profile for $1 \leqslant j \leqslant L$ and for any excited state $|\psi_r^{\pm}\rangle = \prod_{n=1}^{r} b_{k_n} |v^{\pm}\rangle$ with $k_n \neq 0$ is given by

$$\langle \psi_r^{\pm} | \sigma_j^z | \psi_r^{\pm} \rangle = \langle \mathrm{vac} | \sigma_j^z | \mathrm{vac} \rangle + \mathrm{i} \sum_{n=1}^{r} [(\phi_{k_n}^-)_j^+ (\phi_{k_n}^+)_j^- - (\phi_{k_n}^+)_j^+ (\phi_{k_n}^-)_j^-] \tag{B.1}$$

where

$$\langle \mathrm{vac} | \sigma_j^z | \mathrm{vac} \rangle = -\mathrm{i} \langle \mathrm{vac} | \tau_j^+ \tau_j^- | \mathrm{vac} \rangle = -\mathrm{i} \sum_{k=0}^{L+1} (\phi_k^-)_j^+ (\phi_k^+)_j^-. \tag{B.2}$$

Before turning to the profiles for the boundaries in table 1, consider the case $\alpha_z = \beta_z = 0$. According to [1] it is always possible to chose the eigenvectors $(\phi_k^{\pm})$ such that the RHS of (B.1) and (B.2) vanishes for $0 < j < L + 1$ (see the equations (2.38) and (2.40) in [1]). In this case the profiles for all the states $|\psi_r^{\pm}\rangle$ vanish identically. Thus the profile for the ground state of H vanishes also if it is non-degenerate. The partition functions obtained in [6] show that for $L \gg 1$ this is the generic case. Therefore we considered only cases with at least one diagonal boundary term. If the ground state of H is degenerate one has also to consider linear combinations of the states $|\psi_r^{\pm}\rangle$ which correspond to ground states H.

For the cases given in table 1 the polynomial $p(x^2)$ factorizes into cyclotomic polynomials. This enables us to compute the eigenvectors $(\phi_k^{\pm})$ exactly on the finite chain, as explained in [1]. The explicit computations are cumbersome but straightforward and will therefore not be given.

For all cases in table 1 there appears an additional zero mode on top of the spurious mode which does not give a contribution to the RHS of (B.1). Hence the profiles for the two states $|v^+\rangle$ and $b_z|v^-\rangle$, where b_z denotes the creation operator corresponding to the additional zero mode, are identical. One of these states is an element of the (+, +) sector and corresponds to the ground state of H. However, we do not have to know which one, since we are only interested into the profile (note that (A.10) is not applicable, due to the zero mode). Hence in the following we may assume the state $|v^+\rangle$ to be in the (+, +)-sector.

For the cases a, b, c and d with L even no complications arise. The ground state of H is non-degenerate and using the expressions for the $(\phi_k^{\pm})$ in (B.2) leads to a geometric series for each case. Performing the computations yields (11)–(13) and (15).

For case d with L odd the ground state is twofold degenerate, since here two zero modes appear on top of the spurious zero mode. The non-vanishing components of the respective eigenvectors are given by

$$(\phi^{\pm}_{z_1})^{-}_0 = 1 \qquad (\phi^{\pm}_{z_1})^{+}_{L+1} = \pm \mathrm{i} \tag{B.3}$$

and

$$(\phi^{+}_{z_2})^{-}_j = -\mathrm{i}(\phi^{+}_{z_2})^{+}_j = \frac{(-\mathrm{i})^j}{\sqrt{L}} \begin{cases} \mathrm{i} & \text{for} \quad j \text{ even} \\ 1 & \text{for} \quad j \text{ odd} \end{cases} \tag{B.4}$$

where $0 < j \leqslant L$ and $(\phi^{-}_k)^{\pm}_j = \pm(\phi^{+}_k)^{\pm}_j$. In this case we computed the profiles for the two states $|v^+\rangle$ and $b_{z_2}b_{z_1}|v^+\rangle$. This leads to (14) where one has to choose the $-$ sign for the profile of $|v^+\rangle$ and the + sign for the profile of $b_{z_2}b_{z_1}|v^+\rangle$.

However, the computations for case e and the boundary terms (50) are more involved. It is convenient to use the parameter $s = \mathrm{e}^{-2\xi}$ where ξ has been introduced in (50) instead of δ being used in table 1. For odd values of L we have obtained

$$\langle \sigma^z_j \rangle = \frac{\varsigma_j}{\sqrt{s}L} - \frac{1-s}{1-s^L} s^{j-1} \tag{B.5}$$

where

$$\varsigma_j = \sum_{k=1}^{N} \frac{x_k^{2j-3} + x_k^{-2j+3} - x_k^{2j-1} - x_k^{-2j+1} + s(x_k^{2j+1} + x_k^{-2j-1} - x_k^{2j-1} - x_k^{-2j+1})}{1/s + s - x_k^2 - 1/x_k^2} \tag{B.6}$$

with $x_k = \mathrm{e}^{\mathrm{i}\frac{k\pi}{L}}$ and $N = (L-1)/2$. This expression simplifies to a geometric series for $s = 1$. Straightforward computation yields (15) as for case d with L even. We have not been able to compute this expression for $s \neq 1$.

As for case d with L odd, there appear two zero modes on top of the spurious zero mode if we take L even. The non-vanishing components of the corresponding eigenvectors for the first zero mode are again given by (B.3) whereas for the second zero mode they read

$$(\phi^{+}_{z_2})^{-}_j = -\mathrm{i}(\phi^{+}_{z_2})^{+}_j = \mathrm{i}^j \left(\frac{2}{L(1+s)}\right)^{1/2} \begin{cases} \mathrm{i} & \text{for} \quad j \text{ even} \\ -\sqrt{s} & \text{for} \quad j \text{ odd} \end{cases} \tag{B.7}$$

where $0 < j \leqslant L$ and $(\phi^{-}_k)^{\pm}_j = \pm(\phi^{+}_k)^{\pm}_j$. Again we computed the profiles for the two states $|v^+\rangle$ and $b_{z_2}b_{z_1}|v^+\rangle$. Labelling the profile for the state $|v^+\rangle$ by a $-$ sign and the profile for the state $b_{z_2}b_{z_1}|v^+\rangle$ by a + sign, we have obtained

$$\langle \sigma^z_j \rangle_{\pm} = \frac{\varsigma_j}{\sqrt{s}L} - \frac{1-s}{1-s^L} s^{j-1} \pm \frac{2}{L(1+s)} \begin{cases} 1 & \text{for} \quad j \text{ even} \\ s & \text{for} \quad j \text{ odd} \end{cases} \tag{B.8}$$

where ς is again given by (B.6) as for L odd, but with $N = L/2 - 1$. Choosing $s = 1$ allows for the computation of the sum in (B.6) and yields (14) as for case d with L odd.

Although our results on the finite chain are restricted to $s = 1$, one can show that in the continuum limit ($z = j/L$ fixed, $L \to \infty$) ς_j is given by

$$\varsigma_j = \frac{(-1)^j}{1/s+1} \frac{1}{\sin(\pi z)} \tag{B.9}$$

for L odd and by

$$\varsigma_j = \frac{(-1)^j}{1/s+1} \cot(\pi z) \tag{B.10}$$

for L even. Plugging this into (B.8) and (B.5) respectively results in the equations (18) and (19). Note that the exponential contributions in (B.5) and (B.8) vanish in the continuum limit.

The profile in the limit $L \to \infty$, j fixed, leading to (20), may also be computed. In this limit the quantity ς_j/L appearing in (B.5) and (B.8) can be represented as an integral, i.e.

$$\varsigma_j^\infty = \lim_{L\to\infty} \frac{\varsigma_j}{L} = \frac{2}{\pi}\int_0^{\frac{\pi}{2}} \frac{\cos((2j-3)t) - (s+1)\cos((2j-1)t) + s\cos((2j+1)t)}{1/s + s - 2\cos(2t)}\,\mathrm{d}t. \tag{B.11}$$

This integral can be calculated exactly in terms of hypergeometric functions. We obtained

$$\varsigma_j^\infty = \frac{2}{\pi}\left[\frac{(-1)^j}{2j-1} - (-1)^j\left(\frac{1}{s}-1\right)\frac{F(1,1/2+j;3/2+j;-1/s)}{2j+1}\right] \qquad \text{for} \quad s>1 \tag{B.12}$$

$$\sim \frac{2}{\pi}\left[\frac{(-1)^j}{j}\frac{s}{1+s}\right] + \mathrm{O}(j^{-2}) \tag{B.13}$$

and

$$\varsigma_j^\infty = \frac{2}{\pi}\left[\frac{(-1)^j}{2j-1} - (-1)^j(1-s)\frac{F(1,1/2-j;3/2-j;-s)}{2j-1}\right] \qquad \text{for} \quad 0<s<1 \tag{B.14}$$

$$\sim \frac{2}{\pi}\left[\frac{(-1)^j}{j}\frac{s}{1+s} + \frac{\pi(1-s)}{2}s^{j-1/2}\right] + \mathrm{O}(j^{-2}). \tag{B.15}$$

For the asymptotic expansions of the hypergeometric functions see [17]. Using these results in (B.8) and (B.5) gives for even and odd values of L

$$\langle\sigma_j^z\rangle = \frac{(-1)^j}{\pi\cosh\xi}j^{-1} + \cdots. \tag{B.16}$$

Using $\mathrm{e}^\xi = \sqrt{2}\alpha_z$ yields (20). Note that the exponential contributions in (B.8) and (B.5) (which, in the limit in question, are present only for $0<s<1$) are cancelled by the exponential part in (B.15).

We have also considered the profile for a state where the massive fermion is excited, i.e. $|\xi\rangle = b_\xi b_z|v^+\rangle$ for L odd respectively $|\xi\rangle = b_\xi b_{z_1}|v^+\rangle$ for L even (there are two zero modes for L even, where the one labelled by z_1 gives no contribution to the profile (B.1)). Using (B.1), (B.16) and the explicit expressions of the eigenvectors $(\phi_\xi^\pm)$ corresponding to the massive fermion, i.e.

$$(\phi_\xi^+)_j^- = -\mathrm{i}(\phi_\xi^+)_j^+ = \mathrm{i}(-1)^j\left(\frac{1-\mathrm{e}^{-2\xi}}{1-\mathrm{e}^{-2\xi L}}\right)^{1/2}\mathrm{e}^{-2\xi(j-1)} \tag{B.17}$$

where $0<j<L+1$ and $(\phi_\xi^-)_j^\pm = \pm(\phi_\xi^+)_j^\pm$, yields (51) for $\xi>0$ ($s<1$).

Note that for $\xi<0$ ($s>1$) and j fixed the vector components (B.17) vanish as L goes to infinity and the profile for the excited state $|\xi\rangle$ is equal to the ground-state profile given in (B.16). By symmetry (see (50)) this yields the profile near the right-hand boundary for the case $\xi>0$ ($s<1$), i.e. equation (52).

The $U(1)$ charge, i.e. the projection of the total spin onto the z-axis, of the state $|\xi\rangle$ can be computed using the explicit expressions of the $(\phi_k^\pm)$ and summing over j in (B.1) and (B.2) before summing over k (in this way the computation can be performed exactly on the finite chain, independently of the value of s). This yields 0 for L even and $\frac{1}{2}$ for L odd as stated in section 5.2.

Appendix C. Calculation of the σ_j^x-profiles

In this appendix we are going to derive our exact results for the σ_j^x-profiles for the two cases from table 2, i.e. equations (22), (25) and (26). Furthermore we are going to explain how we have obtained the profiles (54) and (55) corresponding to the boundary excitation for the boundary terms in (53) with $\xi_\beta = -\xi_\alpha$.

We have shown in [1] how to compute the expectation values of the σ_j^x-operator in terms of Pfaffians. Here we will only consider cases where diagonal boundary terms are absent (see table 2 and (53)). This enables us to represent $\langle\sigma_j^x\rangle$ in terms of the determinant of a $j \times j$ matrix [1], i.e.

$$\langle v^+|\sigma_j^x|v^+\rangle = f_{0j}\begin{vmatrix} \langle\tau_0^-\tau_1^+\rangle & \langle\tau_0^-\tau_1^-\rangle & \langle\tau_0^-\tau_3^+\rangle & \cdots \\ \langle\tau_2^+\tau_1^+\rangle & \langle\tau_2^+\tau_1^-\rangle & \langle\tau_2^+\tau_3^+\rangle & \cdots \\ \langle\tau_2^-\tau_1^+\rangle & \langle\tau_2^-\tau_1^-\rangle & \langle\tau_2^-\tau_3^+\rangle & \cdots \\ \vdots & \vdots & \vdots & \ddots \end{vmatrix} \tag{C.1}$$

where $f_{0j} = -\mathrm{i}$ for odd values of j and $f_{0j} = 1$ for even values of j. The expectation values of the basic contractions of pairs are given by

$$\langle\tau_i^\mu\tau_j^\nu\rangle = \sum_{k=0}^{L+1}(\phi_k^-)_i^\mu(\phi_k^+)_j^\nu. \tag{C.2}$$

The profiles for the excited states

$$|r\rangle = \prod_{j=1}^{r} b_{k_j}|v^{(-1)^r}\rangle \tag{C.3}$$

are also given by the RHS of (C.1) if one exchanges the $\langle\tau_i^\mu\tau_j^\nu\rangle$ in (C.1) by

$$\langle\tau_i^\mu\tau_j^\nu\rangle_r = \langle\tau_i^\mu\tau_j^\nu\rangle + \sum_{l=1}^{r}[(\phi_{k_l}^+)_i^\mu(\phi_{k_l}^-)_j^\nu - (\phi_{k_l}^-)_i^\mu(\phi_{k_l}^+)_j^\nu]. \tag{C.4}$$

We will start with our computations for case g from table 2 and will then turn to case f from table 2. Afterwards we will consider the boundary terms (53). Again it is possible to solve the eigenvalue equation (A.2) exactly [1]. As for the case of the σ_j^z-profiles we will not give the explicit expressions for the eigenvectors $(\phi_k^\pm)$. They have been obtained as explained in [1]†.

Appendix C.1. Case g

We will first show how to derive equation (26). Afterwards we will compute the function $f(j, L)$ in (26) in the limit $L \to \infty$, $j \gg 1$. Using (26) this yields (25).

It turns out that for our purpose it is convenient to consider the Hamiltonian H_{long} in a different basis, i.e. we consider the Hamiltonian

$$H'_{\mathrm{long}} = U_n H_{\mathrm{long}} U_n^{-1} \tag{C.5}$$

where U_n is given by

$$U_n = \begin{pmatrix} 1 & 0 \\ 0 & 1 \end{pmatrix} \otimes \bigotimes_{j=1}^{L}\begin{pmatrix} 1 & 0 \\ 0 & \mathrm{e}^{\mathrm{i}\varphi}\Gamma^j \end{pmatrix} \otimes \begin{pmatrix} 1 & 0 \\ 0 & (-1)^n \end{pmatrix} \tag{C.6}$$

and

$$\Gamma = \exp\left(\mathrm{i}\frac{\chi + n\pi}{L+1}\right). \tag{C.7}$$

† The boundary terms (53) correspond to case 10 in the notation of [1].

The σ_j^x profile for any state $|g\rangle$ in the original basis is related to the magnetization profiles for the state $|g'\rangle = U|g\rangle$ via

$$\langle g|\sigma_j^x|g\rangle = \cos\left(\varphi + \frac{\chi + n\pi}{L+1}j\right)\langle g'|\sigma_j^x|g'\rangle + \sin\left(\varphi + \frac{\chi + n\pi}{L+1}j\right)\langle g'|\sigma_j^y|g'\rangle. \tag{C.8}$$

The Hamiltonian in the new basis can still be written in terms of free fermions. Of course the fermion energies are not affected by the transformation. The $L+1$ non-zero fermion energies are given by

$$2\Lambda_k = \sin\left(\frac{2k+1}{L+1}\frac{\pi}{2} - \frac{\chi}{L+1}\right) \tag{C.9}$$

where $1 \leqslant k \leqslant L+1$. Computing the eigenvectors $(\phi_k^{\pm})'(\chi, \varphi)$ in the new basis yields that they are independent from the values of χ and φ and can be given in terms of the vectors $(\phi_k^{\pm})(0,0)$ in the original basis, i.e. for $n \geqslant 0$ we have found

$$(\phi_k^{\pm})'(\chi,\varphi) = (\phi_{k+n}^{\pm})(0,0) \qquad \text{for} \quad 1 \leqslant k \leqslant L+1-n \tag{C.10}$$

$$(\phi_k^{\pm})'(\chi,\varphi) = (\phi_{k+n-(L+1)}^{\mp})(0,0) \qquad \text{for} \quad L+1-n < k \leqslant L+1 \tag{C.11}$$

whereas for $n < 0$

$$(\phi_k^{\pm})'(\chi,\varphi) = (\phi_{k-|n|}^{\pm})(0,0) \qquad \text{for} \quad |n|+1 \leqslant k \leqslant L+1 \tag{C.12}$$

$$(\phi_k^{\pm})'(\chi,\varphi) = (\phi_{L+1+j-|n|}^{\mp})(0,0) \qquad \text{for} \quad 1 \leqslant k < |n|+1. \tag{C.13}$$

Now define for n fixed the state

$$|n\rangle = b_{L+2-n}, \ldots, b_{L+1}|v^{(-1)^n}\rangle \qquad \text{for} \quad n > 0 \tag{C.14}$$

and

$$|n\rangle = b_1, \ldots, b_{|n|}|v^{(-1)^n}\rangle \qquad \text{for} \quad n < 0. \tag{C.15}$$

For $n = 0$ define $|0\rangle = |v^+\rangle$. The expectation values in the new basis may be computed in the same way as in the original basis by exchanging the $(\phi_k^{\pm})$ in (C.4) and (C.2) for the $(\phi_k^{\pm})'$. Using (C.10)–(C.13) yields that the σ_j^x-profiles for the states $|n\rangle$ in the new basis are given by

$$\langle n'|\sigma_j^x|n'\rangle = \langle v^+|\sigma_j^x|v^+\rangle \tag{C.16}$$

where the RHS has to be evaluated in the old basis and for the choice $\chi = \varphi = 0$. In the same way one can show that

$$\langle n'|\sigma_j^y|n'\rangle = \langle v^+|\sigma_j^y|v^+\rangle \tag{C.17}$$

where again the RHS has to be computed in the original basis for the choice $\chi = \varphi = 0$. Since for $\chi = \varphi = 0$ the Hamiltonian H_{long} commutes not only with σ_0^x and σ_{L+1}^x, but also with $\sigma_0^x\sigma_1^x \ldots \sigma_{L+1}^x$, the σ_j^y profile in (C.17) vanishes.

However, we have been interested in the ground-state profiles. Computing the value of η using (A.10) with (C.9) yields $\eta = (-1)^{L+1}$ and hence the state $|n\rangle$ is element of the $(+, (-1)^{L+1+n})$-sector (the excitation of a fermion changes the sector from $(\pm, \epsilon)$ to $(\mp, \epsilon)$ [1]). Which of the states $|n\rangle$ corresponds to the ground state of H may be determined by computing the associated energies using (C.9).

For L odd the ground state of H corresponds to the state $|0\rangle = |v^+\rangle$ if $\chi \neq \pi$. For $\chi = \pi$ the ground state of H is twofold degenerate. We obtain two linear independent ground states by choosing the states $|0\rangle$ and $|-2\rangle$.

For L even and $\chi > 0$ the ground state of H corresponds to $|-1\rangle$ whereas for $\chi < 0$ the ground state corresponds to $|1\rangle$. For $\chi = 0$ the ground state is twofold degenerate and we obtain two linear independent ground states choosing the states $|\pm 1\rangle$. Finally, using (C.8)

and (C.16) with $f(j, L) = \langle v^+|\sigma_j^x|v^+\rangle$ (for the choice $\chi = \varphi = 0$) and $m = n/2$ yields (26) and the values of m as explained in the text.

In order to compute $f(j, L)$ we have calculated the expectation values of the basic contractions of pairs (C.2) using the vectors $(\phi_k^{\pm})(0, 0)$. For $i, j < L + 1$ this results in

$$\langle \tau_i^{\pm} \tau_j^{\pm} \rangle = 0 \qquad \langle \tau_0^{-} \tau_j^{+} \rangle = \sqrt{2} g(j) \tag{C.18}$$

$$\langle \tau_i^{+} \tau_j^{-} \rangle = g(i + j) - g(i - j) \qquad \langle \tau_i^{-} \tau_j^{+} \rangle = g(i + j) + g(i - j) \tag{C.19}$$

where the values of i are always even and the values of j are always odd. Furthermore we have defined

$$g(r) = \frac{-\mathrm{i}}{L + 1} \frac{\sin(r\pi/2)}{\sin(r\pi/(2L + 2))}. \tag{C.20}$$

Using elementary operations on determinants in (C.1) one can show that

$$f(j, L) = (-1)^j \left(\frac{2}{\pi}\right)^j \sqrt{2} \det \mathsf{Q}_j \tag{C.21}$$

where the matrix elements of the $j \times j$-matrix Q_j are given by

$$(\mathsf{Q}_j)_{kl} = \left(\frac{\pi}{2L + 2}\right)^j \left(\sin \frac{(2k - 2l + 1)\pi}{2L + 2}\right)^{-1}. \tag{C.22}$$

The boundary behaviour of the profile (i.e. (25)) is obtained taking the limit $L \to \infty$ of Q_j, which yields

$$\lim_{L\to\infty} \mathsf{Q}_j = \begin{pmatrix} 1 & -1 & -\frac{1}{3} & \cdots & \frac{1}{3-2j} \\ \frac{1}{3} & 1 & -1 & \cdots & \frac{1}{5-2j} \\ \frac{1}{5} & \frac{1}{3} & 1 & \cdots & \frac{1}{7-2j} \\ \vdots & \vdots & \vdots & \ddots & \vdots \\ \frac{1}{2j-1} & \frac{1}{2j-3} & \frac{1}{2j-5} & \cdots & 1 \end{pmatrix}. \tag{C.23}$$

The large-j behaviour of the determinant of this matrix is already known [18]. With (C.21) we obtain for $j \gg 1$

$$f(j, \infty) = (-1)^j A j^{-\frac{1}{4}} + \cdots \tag{C.24}$$

where A is defined by (23). Using (26) this yields (25). The function $f(j, L)$ may also be calculated on the finite chain using (C.22) in (C.21) and computing the determinant numerically.

Appendix C.2. Case f

For this case there exists an additional zero mode in the spectrum. Hence the ground state of H corresponds to $|v^+\rangle$ or to $b_z|v^-\rangle$, but we cannot decide which one, since (A.10) cannot be applied. However, the eigenvectors $(\phi_z^{\pm})$ corresponding to the additional zero mode give no contribution to (C.4) as long as $i, j < L + 1$. Hence the profiles for states $|v^+\rangle$ and $b_z|v^-\rangle$ are identical for $j < L + 1$. Defining

$$f(r) = \cos\left(\frac{r}{2L + 2}\pi\right) g(r) \tag{C.25}$$

where $g(r)$ is already given in (C.20), we have obtained for L odd

$$\langle \tau_i^{\pm} \tau_j^{\pm} \rangle = 0 \qquad \langle \tau_0^{-} \tau_j^{+} \rangle = \sqrt{2} g(j) \tag{C.26}$$

$$\langle \tau_i^{+} \tau_j^{-} \rangle = f(i + j) - f(i - j) \qquad \langle \tau_i^{-} \tau_j^{+} \rangle = g(i + j) + g(i - j) \tag{C.27}$$

where i is always even and j is always odd. For L even we obtain

$$\langle \tau_i^{\pm}\tau_j^{\pm}\rangle = 0 \qquad \langle \tau_0^{-}\tau_j^{+}\rangle = \sqrt{2}f(j) \tag{C.28}$$

$$\langle \tau_i^{+}\tau_j^{-}\rangle = g(i+j) - g(i-j) \qquad \langle \tau_i^{-}\tau_j^{+}\rangle = f(i+j) + f(i-j). \tag{C.29}$$

The expressions (C.26)–(C.29) have the same large-L limit as the respective expressions for case g in (C.18) and (C.19). Thus the behaviour of the ground-state profile near the left-hand boundary is also given by the RHS of equation (C.24) which yields (22).

Appendix C.3.

Here we consider the σ_j^x-profile for the boundaries in (53) with $\xi_\beta = -\xi_\alpha$. In this case there appears a massive fermion with energy $2\Lambda = 2\cosh\xi_\alpha$ (see section 5). Here we are interested into the effect of the excitation of this fermion onto the magnetization profile. For simplicity we use $\xi \equiv \xi_\alpha$ in the following.

We have restricted ourselves to even values of L. Since $\eta = (-1)^{L+1}$ the state $|\xi\rangle = b_\xi|v^-\rangle$ (where by b_ξ we denote the creation operator associated with the massive fermion) lies in the $(+,+)$-sector of the Hilbert space of H_{long} and hence corresponds to an eigenstate of H. For odd values of L the $(+,+)$-sector is given by the excitations of an even number of fermions with respect to the ground state $|v^+\rangle$ and hence the state $|\xi\rangle$ does not correspond to an eigenstate of H for L odd.

A lengthy computation yields the expectation values of the basic contractions of pairs (C.2), i.e.

$$\langle \tau_i^{+}\tau_j^{-}\rangle = g(i+j) - g(i-j) \tag{C.30}$$

$$\langle \tau_i^{-}\tau_j^{+}\rangle = \mathrm{i}\frac{\Xi(i+j)+1}{L+1} + g(i-j) + \frac{2\mathrm{i}\sinh(2\xi)\mathrm{e}^{-(i+j)\xi}}{\mathrm{e}^{-2(L+1)\xi}-1} \tag{C.31}$$

$$\langle \tau_0^{-}\tau_j^{+}\rangle = \frac{\sqrt{2}\alpha_+}{\mathrm{e}^{2\xi}+1}\left(\mathrm{i}\frac{\Xi(j)+1}{L+1} + g(j) + \frac{2\mathrm{i}\sinh(2\xi)\mathrm{e}^{-j\xi}}{\mathrm{e}^{-2(L+1)\xi}-1}\right) \tag{C.32}$$

where $g(r)$ has been defined in (C.20) and

$$\Xi(q) = \sum_{n=1}^{\frac{L}{2}}\left[\mathrm{e}^{2\xi}\cos\left(\frac{q-2}{L+1}n\pi\right) + \mathrm{e}^{-2\xi}\cos\left(\frac{q+2}{L+1}n\pi\right) - 2\cos\left(\frac{q}{L+1}n\pi\right)\right] \tag{C.33}$$

$$\times\left[\cosh(2\xi) - \cos\left(\frac{2n}{L+1}\pi\right)\right]^{-1}. \tag{C.34}$$

For $L\to\infty$ we can rewrite $\frac{\Xi(q)}{L+1}$ in terms of an integral which can be calculated using standard methods. In this limit we may write

$$\langle \tau_i^{+}\tau_j^{-}\rangle = -\frac{2\mathrm{i}}{\pi}\left(\frac{\sin((i+j)\pi/2)}{i+j} - \frac{\sin((i-j)\pi/2)}{i-j}\right) \tag{C.35}$$

$$\langle \tau_i^{-}\tau_j^{+}\rangle = -\frac{2\mathrm{i}}{\pi}\Bigg[\frac{\sin((i-j)\pi/2)}{i-j} + \frac{\sin((i+j)\pi/2)}{i+j}\mathrm{e}^{2\xi}$$

$$-2\sinh(2\xi)\mathrm{e}^{-(i+j)\xi}\left(\sum_{m=0}^{\frac{i+j-1}{2}}\frac{(-1)^m\mathrm{e}^{(2m+1)\xi}}{2m+1} - \arctan(\mathrm{e}^{\xi})\right)\Bigg] \tag{C.36}$$

$$\langle \tau_0^{-}\tau_j^{+}\rangle = -\frac{2\sqrt{2}\alpha_+\mathrm{i}}{\mathrm{e}^{2\xi}+1}\Bigg[\frac{\sin(j\pi/2)}{j}(1+\mathrm{e}^{2\xi})$$

$$-2\sinh(2\xi)\mathrm{e}^{-j\xi}\left(\sum_{m=0}^{\frac{j-1}{2}}\frac{(-1)^m\mathrm{e}^{(2m+1)\xi}}{2m+1} - \arctan(\mathrm{e}^{\xi})\right)\Bigg]. \tag{C.37}$$

We used these expressions for the numerical calculation of the determinant in (C.1) for $j = 1, 2, \ldots, 100$. We have chosen 48 different values of ξ in the range between -4.0 and 4.0. Numerical extrapolation yields

$$\langle v^+|\sigma_j^x|v^+\rangle \sim (-1)^j A j^{-1/4} \tag{C.38}$$

where the numerical value of A is given by the RHS of (9) with an accuracy of the order of 10^{-13}.

As already mentioned above here we are interested into the profile of the state where the massive fermion is excited with respect to $|v^-\rangle$. The eigenvectors $(\phi_\xi^\pm)$ associated with the massive fermion are given by

$$(\phi_\xi^+)_0^- = \frac{-\alpha_+}{\cosh\xi}\Big/\rho \quad (\phi_\xi^+)_0^+ = 0 \tag{C.39}$$

$$(\phi_\xi^+)_j^- = \begin{cases} -\sqrt{2}\exp((1-j)\xi)/\rho & \text{for} \quad j \text{ even} \\ 0 & \text{for} \quad j \text{ odd} \end{cases} \tag{C.40}$$

$$(\phi_\xi^+)_j^+ = \begin{cases} 0 & \text{for} \quad j \text{ even} \\ \mathrm{i}\sqrt{2}\exp((1-j)\xi)/\rho & \text{for} \quad j \text{ odd} \end{cases} \tag{C.41}$$

$$(\phi_\xi^+)_{L+1}^+ = \frac{\mathrm{i}\beta_+}{\cosh\xi}\exp((1-L)\xi)/\rho \tag{C.42}$$

where

$$\rho = \sqrt{\frac{\mathrm{e}^{-2L\xi} - \mathrm{e}^{2\xi}}{\sinh(2\xi)}} \tag{C.43}$$

and $(\phi_k^-)_j^\mu = (-1)^j(\phi_k^+)_j^\mu$. In the case $\xi < 0$ this mode does not contribute to (C.4) in the limit $L \to \infty$, since (C.43) diverges, i.e.

$$\langle\xi|\sigma_j^x|\xi\rangle \sim (-1)^j A j^{-1/4} \qquad \text{for} \quad \xi < 0. \tag{C.44}$$

This changes for $\xi > 0$. We assumed the following behaviour of the profile:

$$\langle\xi|\sigma_j^x|\xi\rangle \sim (-1)^{j+1} A(1 - c\mathrm{e}^{-j\eta}) j^{-1/4}. \tag{C.45}$$

Using (C.35)–(C.37) and (C.39)–(C.43) in (C.4) we computed the profile for $j = 1, 2, \ldots, 100$ for 24 different values of ξ in the range between 0 and 4. The values of c and η have been computed using numerical extrapolation by considering the quantity

$$\ln\left(1 + \frac{\langle\xi|\sigma_j^x|\xi\rangle}{\langle v^+|\sigma_j^x|v^+\rangle}\right) \sim \ln c - j\eta. \tag{C.46}$$

Our results have confirmed our assumption (C.45) and the numerical estimates from our extrapolations suggest

$$c = 2\mathrm{e}^{(-1)^j\eta} \qquad \eta = 2\xi \tag{C.47}$$

which yields (54). The largest deviation of the extrapolated values for c and η from (C.47) has been of the order of 10^{-11}. We omit any tables on this. Computing the profile for $\xi > 0$ near the right-hand boundary is equivalent to the computation of the profile near the left-hand boundary for $\xi < 0$ (see (53)), which is given by (C.44). This yields (55).

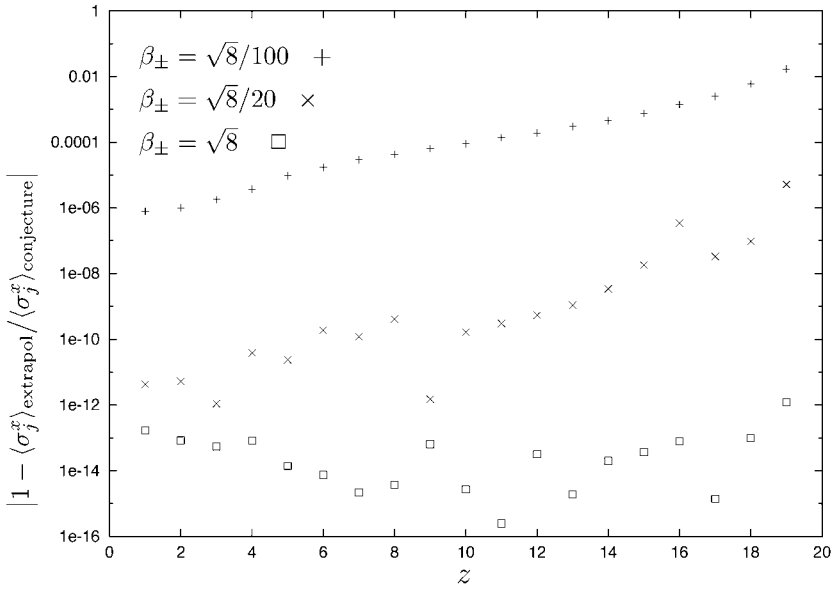

Figure D1. The absolute value of the relative deviation of the extrapolated profile $\langle\sigma_j^x\rangle_{\text{extrapol}}$ from our conjecture (32) for the boundaries (28). The extrapolated profiles have been obtained from finite-size data for lattice lengths $L = 20, 60, \ldots, 700$.

Appendix D. Numerical verification of the conjectures in section 3

We have verified our conjectures (31)–(35) for the continuum limit of the magnetization profiles for the boundary terms (27)–(30). In order to do so, we have used numerical diagonalization to obtain the vectors $(\phi_k^{\pm})$ (see (A.2)) numerically and used (B.1) and (C.1) to obtain the profiles of σ_j^z and σ_j^x respectively on the finite chain. Notice that (C.1) is only valid if $\alpha_z = \beta_z = 0$ and cannot be applied to compute the σ_j^x profile for the boundary terms (30). In this case we made use of the determinant representation (10.14) in [1] of the Pfaffian which determines the profiles.

We computed the profiles on finite lattices with $L = 20, 60, 100, \ldots$ and $L = 21, 63, 105, \ldots$, where the maximum value of L has been chosen in the range of 500–700. For each type of boundary in (27)–(30) we have used 30–50 different values of the respective free parameters.

The values obtained on the finite lattice have been extrapolated to $L = \infty$ for $z = j/L$ fixed using the BST algorithm, where $z = \frac{n}{20}$ for L even and $z = \frac{n}{21}$ for L odd with $n \in \mathbb{N}$.

As already mentioned in the text, the relative deviation of our numerical results from the conjectures is typically of the order of 10^{-12}–10^{-7}. In general the accuracy of our computations depends on the choice of the parameters in (27)–(30) and we have searched for regions in the parameter space where the accuracy of our computations breaks down. We found that this is the case for small values of $\alpha_\pm$ and $\beta_\pm$ in (28) and in (29) and (30). As an example figure D1 shows the relative deviation of the extrapolated σ_j^x-profile for the DN boundary condition (28) with $\alpha_z = 0$ from the exact expression (32) for $\beta_\pm = \sqrt{8}, \sqrt{8}/20, \sqrt{8}/100$ and for even values of L, where we have used finite-size data from $L = 20$ up to 700. The deviations are always in the range of the accuracy of the extrapolations. Hence we avoid any error bars.

The behaviour illustrated in figure D1 is not unexpected, since the vanishing of a non-diagonal boundary term implies a sudden change of the respective boundary condition on the free boson from Neumann to Dirichlet. For the boundaries in question this change implies that the σ_j^x profile vanishes exactly even on the finite chain (the Hamiltonian H commutes with $\sigma_1^z\sigma_2^z\ldots\sigma_L^z$ for $\beta_\pm = 0$ and the ground state of H is non-degenerate). Since the profiles on the finite chain are smooth functions of all parameters appearing in the Hamiltonian, the deviation of the finite-size data from the profile (32) we conjectured for the case $\beta_\pm \neq 0$ in the continuum limit (which does not depend on the value of $\beta_\pm$) increases as $\beta_\pm$ goes to zero. Assuming that our conjecture is correct, it is not surprising that the accuracy of our extrapolations decreases simultaneously.

References

[1] Bilstein U and Wehefritz B 1999 *J. Phys. A: Math. Gen.* **32** 191
[2] Tjon J A 1970 *Phys. Rev.* B **2** 2411
[3] Jordan P and Wigner E 1928 *Z. Phys.* **47** 631
[4] Burkhardt T W and Xue T 1991 *Phys. Rev. Lett.* **66** 895
[5] Burkhardt T W and Xue T 1991 *Nucl. Phys.* B **354** 653
[6] Bilstein U 2000 *J. Phys. A: Math. Gen.* **33** 4437
(Bilstein U 2000 *Preprint* cond-mat/0002162)
[7] Lieb E, Schultz T and Mattis D 1961 *Ann. Phys., NY* **16** 407
[8] McCoy B M 1968 *Phys. Rev.* **173** 531
[9] Fisher M E and de Gennes P G 1978 *C. R. Acad. Sci., Paris* B **287** 207
[10] Cardy J L 1990 *Phys. Rev. Lett.* **65** 1443
[11] Alcaraz F C, Baake M, Grimm U and Rittenberg V 1989 *J. Phys. A: Math. Gen.* **22** L5
[12] Affleck I 1998 *J. Phys. A: Math. Gen.* **31** 2761
[13] Skorik S and Saleur H 1995 *J. Phys. A: Math. Gen.* **28** 6605
[14] Glaisher J W L 1894 *Messenger Math.* **24** 1
[15] Alcaraz F C, Baake M, Grimm U and Rittenberg V 1988 *J. Phys. A: Math. Gen.* **21** L117
[16] Ameduri M, Konik R and LeClair A 1995 *Phys. Lett.* B **354** 376
[17] Luke Y L 1969 *The Special Functions and Their Approximations* (New York: Academic)
Watson G N 1918 *Trans. Camb. Phil. Soc.* **22** 277
[18] McCoy B M and Wu T T 1973 *The Two Dimensional Ising Model* (Cambridge, MA: Harvard University Press) pp 261–4